AGU PUBLICATIONS

Geophysical Research Letters

RESEARCH LETTER
10.1002/2014GL059385

Key Points:
- Lattice thermal conductivity of MgSiO3 at high P and T was calculated using DFT
- Lower mantle radiative and conductive heat transport was assessed
- Thermal conductivity of lower mantle is low and insensitive to P and T

Supporting Information:
- Readme
- Figures S1 to S6

Correspondence to:
A. Kavner,
akavner@ucla.edu

Citation:
Tang, X., M. C. Ntam, J. Dong, E. S. G. Rainey, and A. Kavner (2014), The thermal conductivity of Earth's lower mantle, *Geophys. Res. Lett.*, *41*, 2746–2752, doi:10.1002/2014GL059385.

Received 22 JAN 2014
Accepted 21 MAR 2014
Accepted article online 25 MAR 2014
Published online 16 APR 2014

The thermal conductivity of Earth's lower mantle

Xiaoli Tang[1], Moses C. Ntam[2], Jianjun Dong[2], Emma S. G. Rainey[1], and Abby Kavner[1]

[1]Earth, Planetary and Space Sciences Department, UCLA, Los Angeles, California, USA, [2]Physics Department, Auburn University, Auburn, Alabama, USA

Abstract We assess the thermal conductivity of the Earth's lower mantle anchored on our first-principles calculations of lattice thermal conductivity of $MgSiO_3$ perovskite. Our calculations agree with measurements of iron-free perovskite at ambient conditions and show a lower pressure dependence compared with other recent calculations. In addition, we show that the effect of iron on the lattice thermal conductivity of silicate perovskite is likely to be small at high temperatures. To provide an assessment of thermal conductivity throughout the lower mantle, we reevaluate existing high-pressure optical absorption data to constrain an upper bound radiative contribution to diffusive heat transfer and examine a composite model for combining thermal conductivity of oxide and perovskite phases in the lower mantle. We find that the overall thermal conductivity of the lower mantle is approximately constant between 2.5 and 3.5 W/m/K. These values imply that the mantle has a blanketing effect on heat flow across the core-mantle boundary.

1. Introduction

The chemical and physical behavior of the Earth's core-mantle boundary system governs the large-scale thermochemical evolution of the entire Earth. Heat flux across this thermal boundary layer is described by Fourier's law of heat conduction, $J_{CMB} = -\kappa_{LM}\nabla T$, where the temperature gradient ∇T is given by the temperature difference between the bottom of the convecting mantle and the top of the outer core divided by the average width of the thermal boundary layer, and κ_{LM} is the thermal conductivity of the lower mantle. Uncertainties in all of these values lead to a wide range of estimates—roughly 5 to 15 terawatts—of total heat flow across the core-mantle boundary [*Anderson*, 2007; *Buffett*, 2002; *Lay et al.*, 2008]. This range is permitted within the total surface heat flux generally inferred to be ~44 TW [*Pollack et al.*, 1993], while lower values have been proposed and debated [*Hofmeister and Criss*, 2005; *Von Herzen et al.*, 2005]. The uncertainties in the heat flux across the core-mantle boundary allow a broad range of models describing the thermal and chemical evolution of the whole Earth, including variations in the convection style of the mantle which drives surface plate tectonics at the surface and the evolution of the inner core/outer core system which helps drive generation of the magnetic field.

The lower mantle thermal conductivity is especially ill constrained due to the difficulty in measuring thermal transport properties of materials at the relevant high pressures and temperatures. Measurements made at lower pressures and temperatures require large extrapolations to lowermost mantle conditions, and these extrapolations are based on uncertain physical models, many of them based on the behavior of much simpler crystalline structures such as MgO [*Hofmeister*, 2007; *Dekura et al.*, 2013; *Manthilake et al.*, 2011; *Osako and Ito*, 1991]. As a result, there are large discrepancies among current assessments for lattice thermal conductivity for the predominant deep Earth minerals, i.e., iron (Fe)-bearing magnesium silicate perovskite ($MgSiO_3$-pv) [*Dekura et al.*, 2013; *Haigis et al.*, 2012; *Manthilake et al.*, 2011; *Ohta et al.*, 2012; *Osako and Ito*, 1991] and periclase (MgO) [*de Koker*, 2009, 2010; *Katsura*, 1997; *Stackhouse et al.*, 2010; *Tang and Dong*, 2009, 2010]. In addition, disagreement over the relative importance of lattice thermal conductivity versus any radiative contribution adds to the overall uncertainty for lower mantle heat flow [*Goncharov et al.*, 2008; *Keppler et al.*, 2008].

In this report, we present a comprehensive assessment of the thermal conductivity of the lower mantle, anchored by new first-principles calculations of the lattice thermal conductivity of $MgSiO_3$-pv high pressures and temperatures. We calculate the effect of iron substitution on the thermal conductivity of both $MgSiO_3$-pv and on MgO. To calculate the radiative contribution, we reanalyze two existing high-pressure optical absorption data sets from *Goncharov et al.* [2008] and *Keppler et al.* [2008]. Finally, we use a composite model to provide our estimate of aggregate lower mantle thermal conductivity as a function of pressure and temperature and elucidate some of the implications for lower mantle heat flow.

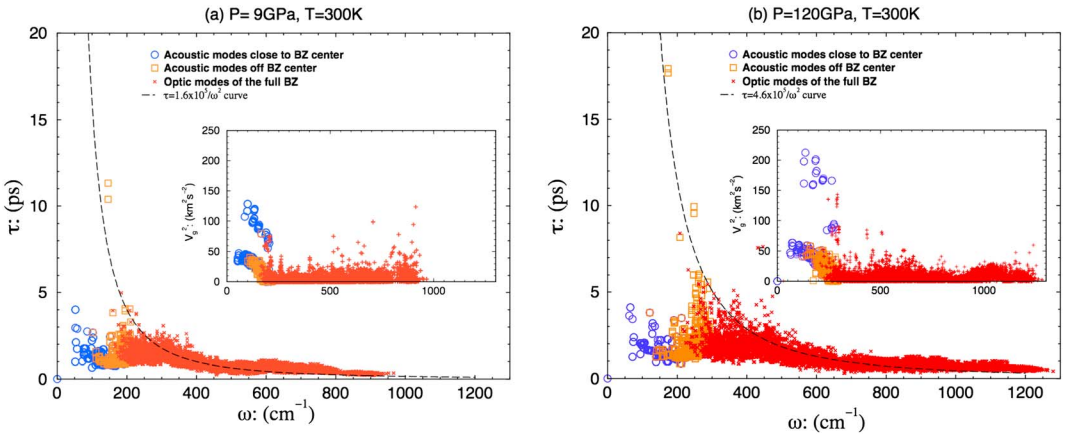

Figure 1. Calculated phonon lifetimes, τ, at 300 K as a function of phonon frequency (ω) for the complete set of 23,040 phonon modes over an $8 \times 8 \times 6$ *k* point grid of the reciprocal space Brillouin zone (BZ) of a 20 atom $MgSiO_3$ perovskite unit cell. The optic modes are shown as red plus symbols; the acoustic modes close to the BZ center are shown as blue circles, and acoustic modes far from the BZ center are shown as orange squares. (a) Values at 9 GPa and (b) values at 120 GPa. The insets show the square of the group velocity as a function of phonon frequency.

2. Computational Methods: Peierls-Boltzmann Kinetic Phonon Transport Model for Lattice Thermal Conductivity

We adopted similar first-principles computational methodologies to those reported in previous studies of MgO periclase [*Tang and Dong*, 2009, 2010], and additional details are provided in the supporting information. Lattice thermal conductivity (κ_{latt}) is calculated based on the theoretical framework of the kinetic phonon gas theory using the Peierls-Boltzmann transport equation and the single-mode excitation approximation

$$\kappa_{latt} = 1/V_{BZ} \times \int_{BZ} \left[\sum_i \left(c_V(k,i) \times {v_g}^2(k,i) \times \tau(k,i)/3\right] dk \quad (1)$$

In this formulation κ_{latt} is expressed as the product of the phonon heat capacity, C_V, the square of the group velocity, V_g, and the phonon lifetime, τ, summed for *i* phonon modes at *k* points in reciprocal space and integrated across the Brillouin zone.

The phonon properties are explicitly calculated using first-principles methods without any empirical fitting. Phonon lifetimes are computed based on the phonon-scattering rates associated with third-order lattice anharmonicity and isotope/mass disorder-induced phonon scattering. Realistic evaluation of phonon lifetimes of individual modes requires an accurate assessment of the number of the conservation-allowed three-phonon configurations, the anharmonic coupling strengths, and the frequencies of the phonons. One advantage of our first-principles method is that the lifetime calculations, our most computationally intensive step, can be carried out in parallel, which allows us to take full advantage of massive parallel supercomputing platforms. More than 2 million CPU hours were required to calculate κ_{latt} of pv-$MgSiO_3$ at 36 *P-T* conditions ranging from ambient to those corresponding to the deep mantle.

3. Calculated Phonon Behavior and Lattice Thermal Conductivity for $MgSiO_3$-pv

Figure 1 shows the calculated phonon lifetimes and the mode group velocities (insets) at two pressures, with symbols differentiating optic modes (plus) and acoustic modes near and far from the Brillouin zone center (blue circles and orange squares, respectively). The acoustic modes close to the Brillouin zone center have the largest group velocities and are strongly pressure dependent. However, in perovskite, unlike MgO, these only account for a small fraction of the phonons responsible for determining the overall thermal transport. The bulk of the phonons have lower group velocities and generally show little pressure dependence—indeed some of the optic phonon modes have velocities that are noticeably lower at 120 GPa than at 9 GPa. Our calculated phonon lifetimes are generally an order of magnitude smaller than those for MgO, and their pressure dependence varies from mode to mode, with the heat-carrying acoustic modes typically the least

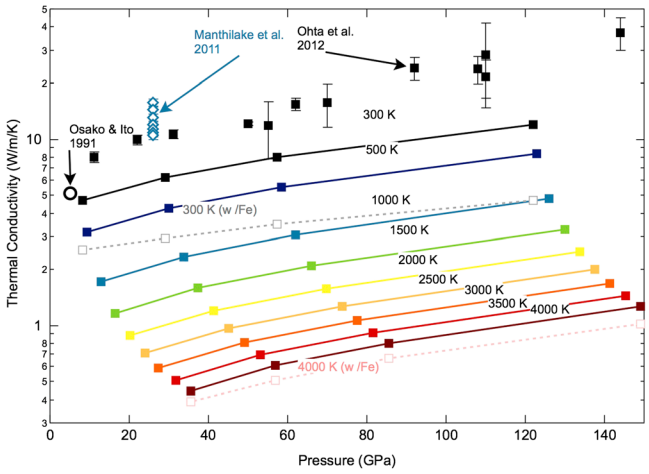

Figure 2. Pressure and temperature dependence of lattice thermal conductivity of $MgSiO_3$ perovskite with experimental measurements. Solid lines: iron-free crystal. Dashed lines: calculations with 12.5% Fe (plotted only at 300 K and 4000 K). Also plotted are experimental data from *Osako and Ito* [1991] on $MgSiO_3$-pv, from *Ohta et al.* [2012] on $MgSiO_3$-pv, and from *Manthilake et al.* [2011] on $(Mg,Fe)SiO_3$ at temperatures from 473 to 1073 K.

pressure sensitive. The optic mode lifetimes scale approximately with $1/\omega^2$ and increase with pressure (Figure 1, plus symbols).

The calculated lattice thermal conductivity of $MgSiO_3$-pv has low values, gradually increases with pressure ($d\log(\kappa_{latt})/dP = 0.02\ GPa^{-1}$) (Figure 2) and decreases with temperature as 1/T. Our calculation at 300 K is in good agreement with some experimental measurements: ~20% lower than the single ambient pressure measurement [*Osako and Ito*, 1991] and ~30% smaller than a recent set of diamond anvil cell measurements [*Ohta et al.*, 2012], but with similar pressure dependence. A third set of measurements performed at ~26 GPa using a multianvil technique reports higher overall values for thermal conductivity and a $T^{-0.43}$ dependence [*Manthilake et al.*, 2011]. Our calculated values for thermal conductivity are much lower than the high values calculated using molecular dynamics approaches [*Haigis et al.*, 2012] and lower than those calculated in *Dekura et al.* [2013] (Figure 3). A detailed comparison between our calculations and those by Dekura et al. show that the calculations for phonon lifetime at the Brilliouin zone center are in good agreement but that Dekura et al. use the empirical relationship correlating phonon lifetime with $1/\omega^2$ to estimate tau away from the zone center. This is at odds with our phonon lifetime calculations demonstrating the failure of the $1/\omega^2$ relationship away from the zone center. As a result, the study by *Dekura et al.* [2013] overestimates phonon lifetimes, and therefore thermal conductivity and its pressure dependence thermal conductivity.

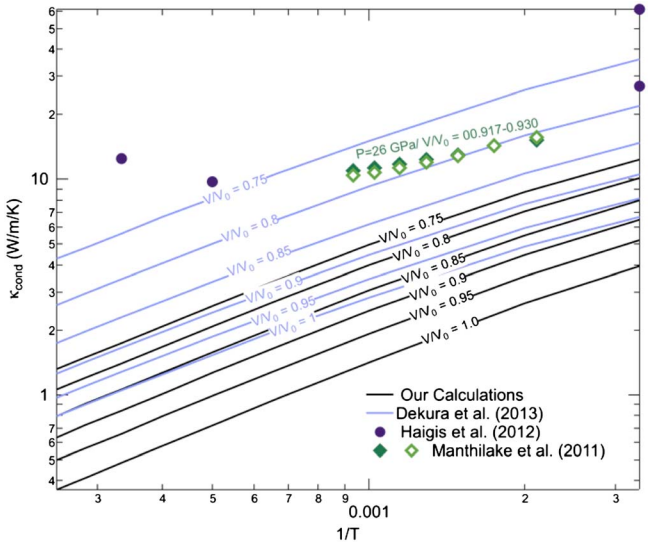

Figure 3. Temperature dependence of thermal conductivity of MgSiO3 perovskite. Our calculations are in black; calculations from *Dekura et al.* [2013] are shown in lavender, and those from *Haigis et al.* [2012] are shown as black cirlcles. Measurements of *Manthilake et al.* [2011] are shown as green triangles (measurement uncertainties of ~3% reported by Manthilake et al. are within the size of the symbols).

Our calculated 1/T dependence (Figure 3) is consistent with most physical models for lattice thermal conductivity in insulating crystals [*Klemens*, 1958; *Katsura*, 1997; *de Koker*, 2009, 2010; *Stackhouse et al.*, 2010; *Tang and Dong*, 2010; *Haigis et al.*, 2012; *Dekura et al.*, 2013], and the 1/T dependence is also calculated by the two other computational studies, a molecular dynamics simulation [*Haigis et al.*, 2012] and an additional study also based on density functional theory [*Dekura et al.*, 2013].

4. Lower Mantle Thermal Conductivity

Our computational result shows that high temperatures have a much more stringent effect on reducing lattice thermal conductivity in perovskite than does increasing pressure. Our calculated values result in a lattice thermal

conductivity for $MgSiO_3$-pv to be 1–2 W/m/K at pressures and temperatures corresponding to the lowermost mantle. For context, these values are similar to ambient pressure and temperature thermal conductivities for $CaTiO_3$-perovskite (~4.4 W/m/K) [*Hofmeister*, 2010] and for igneous rocks (~2–5 W/m/K) [*Robertson*, 1988]. To use our results to anchor an estimate for lower mantle conductivity, three additional factors must be considered: (1) the calculated effect of iron impurities on the lattice thermal conductivity of MgO and $MgSiO_3$-pv, (2) possible contributions to the overall thermal conductivity from radiative heat flow in the lower mantle, and (3) the aggregate thermal conductivity behavior of a polyphase lower mantle assemblage.

4.1. Effect of Iron Substitution on Lattice Thermal Conductivity

Iron substitution lowers lattice thermal conductivity via disorder-induced scattering that reduces phonon lifetimes and by generating lower phonon group velocities due to iron's larger mass and weaker chemical bonds. For the purposes of this study, we create an Fe-bearing mineral solid solution with the same force constants and lattice anharmonicity as the Mg end-member, but with additional Mg/Fe mass disorder and heavier average mass ($Mg_{1-x}Fe_x$). This approximation, which ignores electronic bonding changes, gives an upper bound of κ_{latt} for the solid solution. For MgO, we performed a more computationally intensive phonon virtual crystal approximation test for one Fe-bearing ($Mg_{1-x}Fe_x$)O model containing 12.5% low-spin ferrous Fe^{2+} and confirmed that the mass effects are significantly larger than the change of force constants at high temperatures (see supporting information). Our results show that Fe substitution lowers κ_{latt} because of the impurity scattering effect. This effect is greater for MgO, which has a lower thermal resistance to begin with, and greater at lower temperatures. The overall effect at lower mantle conditions is small: the presence of iron lowers the lattice conductivity by less than a few percent (Figure 2).

4.2. Radiative Conductivity in the Lower Mantle

The low κ_{latt} values for perovskite necessitate a reassessment of radiative contributions to the overall thermal conductivity. In the optically thick limit, which is relevant for the Earth's lowermost mantle, heat transfer by radiation can be modeled as a diffusion process [*Siegel and Howell*, 2002; *Rosseland*, 1924], with an effective radiative thermal conductivity given by Rosseland mean approximation

$$Q_{rad} = -\frac{16\sigma n^2 T^3}{3\beta_R}\nabla T = -\kappa_{rad}\nabla T \tag{2a}$$

$$\frac{n^2}{<\beta_R>} = \frac{\pi}{4\sigma T^3}\int_0^\infty \frac{n_\lambda^2}{\beta_\lambda}\frac{dI_{b,\lambda}}{dT}d\lambda \tag{2b}$$

Here n is the index of refraction, σ is the Stefan-Boltzmann constant, β_R is the Rosseland mean extinction coefficient, λ is wavelength, n_λ is the spectral index of refraction, β_λ is the spectral extinction coefficient, and $I_{b,\lambda}$ is the Planck blackbody intensity function. We use this approximation to calculate the effective radiative contribution to thermal conductivity using two measurements of spectral optical absorption of perovskite in the diamond anvil cell [*Goncharov et al.*, 2008; *Keppler et al.*, 2008]. Both of these data sets were obtained at ambient temperature with no temperature correction. It is likely that the high temperatures increase optical absorption due to excitement of charge defects to the conduction band, especially for transition-element-bearing minerals in the lower mantle. This serves to render our estimate for κ_{rad} an upper bound. While in the original studies reporting absorption measurements [*Goncharov et al.*, 2008; *Keppler et al.*, 2008] yielded order of magnitude different estimates for radiative conductivity, our consistent treatment shows that they are in good general agreement, with optical absorption behavior showing similar spectral behavior and pressure trends, but differ in magnitude by a factor of 2 to 3. Additional uncertainties in the determination of the radiative contribution to overall thermal conductivity are discussed in the supporting information.

For our overall determination of lower mantle conductivity, we incorporate the average of the two estimates and consider this value to be an upper bound to the radiative contribution to the lower mantle because any consideration of additional scattering defects such as impurities and/or grain boundaries will solely serve to inhibit radiative transfer.

Our resulting estimate of κ_{rad} (Figure 3) is comparable in magnitude with κ_{latt}, but with opposing T dependence. The resulting total thermal conductivity for perovskite is therefore approximately constant as a function of T and depth throughout the lower mantle (Figure 3). Modest temperature perturbations about the geotherm will

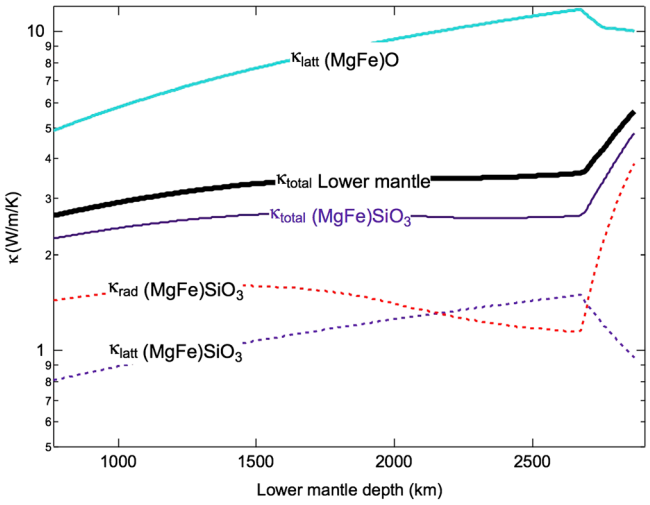

Figure 4. Thermal conductivity calculated down a lower mantle geotherm [*Jeanloz and Morris*, 1986] with a ~250 km thick thermal boundary layer in the lowermost mantle. Lattice thermal conductivity calculated from first principles for Fe-bearing MgO (solid blue line) [*Tang and Dong*, 2009] and Fe-bearing $MgSiO_3$ perovskite (solid purple line, this study). Thin red lines show radiative contribution to thermal conductivity averaged from existing optical absorption estimates [*Goncharov et al.*, 2008; *Keppler et al.*, 2008]. Total radiative plus lattice thermal conductivity of $MgSiO_3$ perovskite is shown as a purple line. Total thermal conductivity of a perovskite plus periclase mantle calculated from the composite model is shown as a thick black line.

increase the radiative contribution while attenuating the lattice contribution. The effect of defects and impurities will tend to lower both the radiative and lattice contributions for the thermal conductivity; therefore, this nearly T independence of total thermal conductivity is a robust outcome of our analysis. A constant value of κ_{LM} will certainly simplify lowermost mantle heat flow models, which are unlikely to show nonlinear behavior except under local and unusual conditions [*Hofmeister and Yuen*, 2007].

4.3. Maxwell-Garnett Composite Model for Averaged Thermal Conductivity

Finally, we determine the total κ_{LM} for a mineralogical model of the lower mantle based on the Maxwell-Garnett effective medium approximation for examining the total conductivity where a minor phase exists as random inclusions within a matrix phase [*Levy and Stroud*, 1997; *Progelhof et al.*, 1976]. As a first-order representation of the lower mantle, we consider a composite model consisting of a matrix of Fe-bearing perovskite with ~20% Fe-bearing oxide existing as isolated inclusions. We perform the calculation by first summing the lattice and radiative contributions for each phase and then combining the two phases in the composite model. Changes in the order of summation, local layering, or texturing of the mineral phases may play a role in either raising or lowering the local aggregate thermal conductivity, but only by a few tens of percent [see supporting information]. Figure 4 shows our best estimate for total κ_{LM} down an estimated average lower mantle geotherm [*Jeanloz and Morris*, 1986], including the effect of a ~150 km thick thermal boundary layer between the convecting lower mantle and the core-mantle boundary. Our best estimate of total thermal conductivity throughout the convecting lower mantle rises gradually from ~2.5 W/m/K just below the transition zone to 3.5 W/m/K at the bottom of the convecting mantle. The local presence of postperovskite within the thermal boundary layer may also alter local thermal conductivity [*Anzellini et al.*, 2013]. While the absolute value of the thermal conductivity of the boundary layer may be uncertain by ~50% because of its sensitivity to variations in composition and mineralogical texture effects such as layering, our analysis shows that the thermal conductivity is approximately constant with variations in pressure and temperature throughout the lower mantle.

5. Implications for the Earth

In the thermal boundary layer above the core, trade-offs in the assumed temperature of the lower mantle and the temperature at the top of the outer core map to values rising from 3.5 W/m/K at the bottom of the convecting mantle to 5.5 W/m/K just above the outermost core. Our new estimate of J_{CMB} is equal to 6 TW (±2 TW), based on an assumption of an average thermal boundary layer (TBL) of 150 km, consistent with seismic observations of the width of this layer in *Hunt et al.* [2012], and a T drop across the core-mantle boundary (CMB) equal to 1400 K, corresponding to a new estimate of the core T in *Hernlund et al.* [2005] and adiabatic behavior in a convecting mantle. Figure 5 illustrates how trade-offs in the assumed values for thickness of the lower mantle TBL and T difference between the convecting mantle and outer core influence estimates of the total heat flux crossing the CMB. Total heat flux of 10 TW is allowable if the average boundary thickness is 100 km. The revised estimate of heat flow is above the geophysically constrained minimum bound of ~4 TW that is

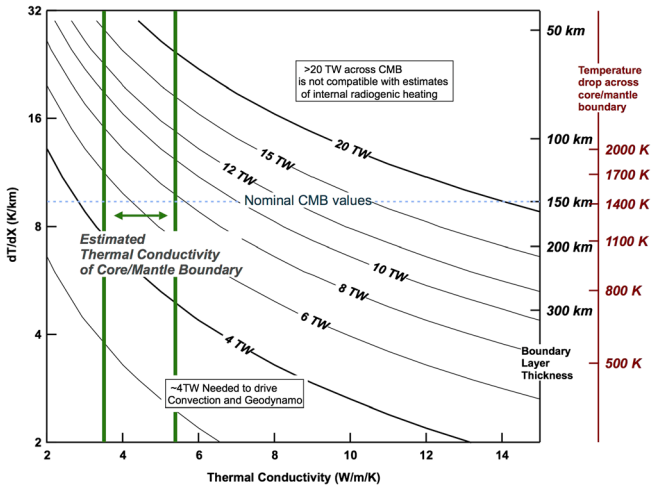

Figure 5. Summaries of trade-offs among the observational constraints used to calculate an average total heat flow across the core-mantle boundary (contoured, labels in terawatts). Vertical solid green lines delineate our newly determined range of estimates for lower mantle thermal conductivity. A horizontal axis shows a reasonable (yet uncertain) value for temperature gradient across the lower mantle thermal boundary layer. The two right-hand axes demonstrate sensitivity of total heat flux to the boundary layer thickness (assuming a constant temperature drop of 1400 K between the outer core and convecting lower mantle [*Anzellini et al.*, 2013]) and to temperature difference between outer core and lower mantle (assuming constant boundary layer thickness of 150 km). Our favored value for total heat flow across the core-mantle boundary is 6 TW, with uncertainties mostly described by the trade-offs documented in Figure 5.

required to permit driving of the core geodynamo and below the geochemically constrained upper bound of ~20 TW bound that is allowed by recent, albeit broad, estimates of radioactive heating in the mantle from *The KamLAND Collaboration* [2011]. Our lower value for heat flux across the core-mantle boundary relaxes some of the constraints on timing of inner core growth [*Buffett*, 2002], while still permitting the geodynamo, and does not pose difficulties in accounting for the global heat balance of the mantle [e.g., *Lay et al.*, 2008; *The KamLAND Collaboration*, 2011].

Our results suggest that the constant variations of the thermal conductivity as a result of lateral variation in T or P will not be significant. However, local changes in modal abundance of minerals, mineral chemistry, Fe content, presence of melt, and/or mechanical texturing may significantly perturb the value of κ_{LM}. Therefore, variations in heat flow across the CMB can be simply mapped directly from variations in either boundary thickness or variations in compositionally sensitive geophysical probes of the lower mantle, such as the ratio of bulk and shear velocities. Based on seismic evidence of distinctly different provinces at the core-mantle boundary, which may be a combination of compositional, textural, and/or phase variations, we estimate that the lateral variability in heat flow along the core-mantle boundary may be significant, up to 50%. Therefore, local variations of the lower mantle thermal conductivity may govern local modes of heat flow at the lower mantle thermal boundary, providing a bottom-up control on the behavior of the convective mantle system.

Acknowledgments
We acknowledge funding from the National Sciences Foundation (NSF) under grant numbers, EAR 0757847 (JD), EAR 0969033 (AK), and EAR 0510914 (AK). J.D. thanks supports by the Thomas and Jean Walter Professorship endowment at Auburn University. Calculations were supported by the NSF through TeraGrid [TG-EAR090031] and the Alabama Supercomputer Authority.

The Editor thanks Anne M. Hofemister for her assistance in evaluating this paper.

References

Anderson, D. L. (2007), *New Theory of the Earth*, Cambridge Univ. Press, New York.
Anzellini, S., A. Dewaele, M. Mezouar, P. Loubeyre, and G. Morard (2013), Melting of iron at Earth's inner core boundary based on fast X-ray diffraction, *Science*, *340*, 464–466, doi:10.1126/science.1233514.
Buffett, B. A. (2002), Estimates of heat flow in the deep mantle based on the power requirements for the geodynamo, *Geophys. Res. Lett.*, *29*(12), 1566, doi:10.1029/2001GL014649.
de Koker, N. (2009), Thermal conductivity of MgO, *Phys. Rev. Lett.*, *103*, 125,902–125,905, doi:10.1103/PhysRevLett.103.125902.
de Koker, N. (2010), Thermal conductivity of MgO periclase at high pressure: Implications for D″ region, *Earth Planet. Sci. Lett.*, *292*, 392–398, doi:10.1016/j.epsl.2010.02.011.
Dekura, H., T. Tsuchiya, and J. Tsuchiya (2013), *Ab initio* lattice thermal conductivity of $MgSiO_3$ perovskite as found in Earth's lower mantle, *Phys. Rev. Lett.*, *110*, 025,904–025,908, doi:10.1103/PhysRevLett.110.025904.
Goncharov, A. F., B. D. Haugen, V. V. Struzhkin, P. Beck, and S. D. Jacobsen (2008), Radiative conductivity in the Earth's lower mantle, *Nature*, *456*, 231–234, doi:10.1038/nature07412.
Haigis, V., M. Salanne, and S. Jahn (2012), Thermal conductivity of MgO, $MgSiO_3$ perovskite and post-perovsite in the Earth's deep mantle, *Earth Planet. Sci. Lett.*, *355–356*, 102–108, doi:10.1016/j.epsl.2012.09.002.
Hernlund, J. W., C. Thomas, and P. J. Tackley (2005), A doubling of the post-perovskite phase boundary and structure of the Earth's lowermost mantle, *Nature*, *434*, 882–886, doi:10.1038/nature03472.
Hofmeister, A. M. (2007), Pressure dependence of thermal transport properties, *Proc. Natl. Acad. Sci. U. S. A.*, *104*, 9192–9197, doi:10.1073/pnas.0610734104.
Hofmeister, A. M. (2010), Thermal diffusivity of oxide perovskite compounds at elevated temperature, *J. Appl. Phys.*, *107*(10), 103,532.
Hofmeister, A. M., and R. E. Criss (2005), Earth's heat flux revised and linked to chemistry, *Tectonophysics*, *395*(3), 159–177.
Hofmeister, A. M., and D. A. Yuen (2007), Critical phenomena in thermal conductivity: Implications for lower mantle dynamics, *J. Geodyn.*, *44*, 186–199, doi:10.1016/j.jog.2007.03.002.

Hunt, S. A., D. R. Davies, A. M. Walker, R. J. Mccormack, A. S. Wills, D. P. Dobson, and L. Li (2012), On the increase in thermal diffusivity caused by the perovskite to post-perovskite phase transition and its implications for mantle dynamics, *Earth Planet. Sci. Lett.*, *319*, 96–103, doi:10.1016/j.epsl.2011.12.009.

Jeanloz, R., and S. Morris (1986), Temperature distribution in the crust and mantle, *Annu. Rev. Earth Planet. Sci.*, *14*, 377–415, doi:10.1146/annurev.ea.14.050186.002113.

Katsura, T. (1997), Thermal diffusivity of periclase at high temperatures and high pressures, *Phys. Earth Planet. Inter.*, *101*, 73–77, doi:10.1016/S0031-9201(96)03223-2.

Keppler, H., L. S. Dubrovinsky, O. Narygina, and I. Kantor (2008), Optical absorption and radiative thermal conductivity of silicate perovskite to 125 Gigapascals, *Science*, *322*, 1529–1532, doi:10.1126/science.1164609.

Klemens, P. G. (1958), Thermal conductivity and lattice vibrational modes, *Solid State Phys.*, *7*, 1–98.

Lay, T., J. Hernlund, and B. A. Buffett (2008), Core-mantle boundary heat flow, *Nat. Geosci.*, *1*, 25–32, doi:10.1038/ngeo.2007.44.

Levy, O., and D. Stroud (1997), Maxwell Garnett theory for mixtures of anisotropic inclusions: Applications to conducting polymers, *Phys. Rev. B*, *56*, 8035–8046, doi:10.1103/PhysRevB.56.8035.

Manthilake, G. M., N. de Koker, D. J. Frost, and C. A. McCammon (2011), Lattice thermal conductivity of lower mantle minerals and heat flux from Earth's core, *Proc. Natl. Acad. Sci. U. S. A.*, *108*, 17,901–17,904, doi:10.1073/pnas.1110594108.

Ohta, K., T. Yagi, N. Taketoshi, K. Hirose, T. Komabayashi, T. Baba, Y. Ohishi, and J. Hernlund (2012), Lattice thermal conductivity of $MgSiO_3$ perovskite and post-perovskite at the core-mantle boundary, *Earth Planet. Sci. Lett.*, *349–350*, 109–115, doi:10.1016/j.epsl.2012.06.043.

Osako, M., and E. Ito (1991), Thermal diffusivity of $MgSiO_3$ perovskite, *Geophys. Res. Lett.*, *18*, 239–242, doi:10.1029/91GL00212.

Pollack, H. N., S. J. Hurter, and J. R. Johnson (1993), Heat flow from the Earth's interior: Analysis of the global data set, *Rev. Geophys.*, *31*, 267–280.

Progelhof, R. C., J. L. Throne, and R. R. Ruetsch (1976), Methods for predicting thermal conductivity of composite systems, *Polym. Eng. Sci.*, *16*, 615–625, doi:10.1002/pen.760160905.

Robertson, E. C. (1988), *Thermal Properties of Rocks*, U.S.G.S. Open file report 88–441, 106 pp., U.S. Geol. Survey, Reston, Va.

Rosseland, S. (1924), Electrical state of a star, *Mon. Not. R. Astron. Soc.*, *84*, 720.

Siegel, R., and J. R. Howell (2002), *Thermal Radiation Heat Transfer*, Taylor & Francis, New York.

Stackhouse, S., L. Stixrude, and B. B. Karki (2010), Thermal conductivity of periclase (MgO) from first principles, *Phys. Rev. Lett.*, *104*, 208,501–208,504, doi:10.1103/PhysRevLett.104.208501.

Tang, X., and J. Dong (2009), Pressure dependence of harmonic and anharmonic lattice dynamics in MgO: A first-principles calculation and implications for lattice thermal conductivity, *Phys. Earth Planet. Inter.*, *174*, 33–38, doi:10.1016/j.pepi.2008.10.003.

Tang, X., and J. Dong (2010), Lattice thermal conductivity of MgO at conditions of Earth's interior, *Proc. Natl. Acad. Sci. U. S. A.*, *107*, 4539–4543, doi:10.1073/pnas.0907194107.

The KamLAND Collaboration (2011), Partial radiogenic heat model for Earth revealed by geoneutrino measurements, *Nat. Geosci.*, *4*, 647–651, doi:10.1038/ngeo1205.

Von Herzen, R., E. E. Davis, A. T. Fisher, C. A. Stein, and H. N. Pollack (2005), Comments on "Earth's heat flux revised and linked to chemistry" by AM Hofmeister and RE Criss, *Tectonophysics*, *409*(1), 193–198.